RSC Advances

ROYAL SOCIETY OF CHEMISTRY

www.rsc.org/advances

Polycrystalline Boron Nitride constructed from hexagonal boron nitride

N. Xu[1,*], J. F. Li[2], B. L. Huang[2], and B. L. Wang[1]

Two classes of structural families of boron nitride allotropes (named as *X*-BNs and *L*-BNs) are proposed to shed light on polycrystalline structure of high pressure *h*-BN. We find that the previously proposed *pct*-BN, *Z*-BN belong to our currently proposed family (*L*-BNs). *X*-BNs are much more stable at zero pressure and more energetically favorable than *L*-BN and *w*-BN. *X*-BNs can be viewed as the mixture of *w*-BN and *c*-BN. Surprisingly, the transition from *h*-BN to *X*-BNs can occur simply through sliding and buckling of BN sheets. The calculated bulk modulus and densities of X-BNs match well with the experimental datas. Our calculations predict that *X*-BNs is a transparent wide band-gap insulator.

[1]*Department of Physics, Yancheng Institute of Technology, Yancheng 224051, China*
[2]*Department of Physics and Materials Science, City University of Hong Kong, Hong Kong SAR, China*
[*] E-mail: nxu@ycit.cn; hyblwang@pub.hy.jsinfo.net

Cubic diamond is the hardest known material. Over the past few decades, scientists have struggled to find materials that are harder and thermally more stable than diamond.[1-4] It was recently reported nano-polycrystalline boron nitrides (BNs) synthesised from hexagonal boron nitride (*h*-BN) at high temperatures, show hardness reaching the same level of indentation hardness as diamond.[5] This kind of polycrystalline BN can be viewed as the mixture of cubic (*c*-) and wurtzite (*w*-) BN. As we all known that *c*-BN is the second hardest known material, and its strength and hardness are well below those of diamond.[6,7] According to the experimental results, there was speculation that *w*-BN may be as hard or harder than diamond. It came as a surprise since *w*-BN and *c*-BN have a similar bond length, elastic moduli, and ideal tensile and shear strength.[8] The recent first-principle calculations show that the vickers' hardness of *w*-BN is lower than that of *c*-BN,[9,10] which conflicts with the theoretical result of Pan et al. in 2009 that *w*-BN possess superior indentation strength that is 58% higher than the corresponding value of diamond.[11] Meanwhile, several hypothetical structures, such as *pct*-BN[9,12,13] and *Z*-BN,[10] are proposed to shed light on the superhard mechanism of polycrystalline BNs. The simulated results show that these BN phases possess even higher enthalpy values and even lower vicker' hardness compared with *c*-BN and *w*-BN. These proposed BN phases are controversial, because their crystal structure differs from the experimental results that polycrystalline BNs consist mainly of *c*-BN and *w*-BN. In addition, Zhi et al recently synthesized and engineered large-scaled BN nanostructures associated with electronic structure measurements.[Zhi 22, Zhi 23] Therefore, it is essential to examine its intrinsic structure to understand the unexpectedly high indentation hardness of polycrystalline BNs.

In experiment, the *c*-BN was synthesized by the direct conversion from *h*-BN under high pressure (5~8GPa) at high temperature (1700~2300°C)[14,15,16] and *w*-BN was synthesized at relatively low temperature (~1300°C).[16,17] Similarly, nano-polycrystalline BNs were synthesized by the direct-conversion method from *h*-BN at high temperatures.[5] *h*-BN consists of stacked layers of BN sheets and held together by weak van der Waals forces, thus the relative slippage between the BN sheets is very easily owing to the lower potential barriers. We find *c*-BN and *w*-BN can be viewed as wrinkle hexagonal BN sheets interconnected regularly (see in figure 1.), and also can be regarded as a distorted (through sliding and buckling of the sheets) form of *h*-BN. Therefore, we suppose that polycrystalline BNs should be constructed from the distorted BN sheets, and have similar crystal structrue to *c*-BN and *w*-BN.

In the present work, we report two families of sp^3-hybridized superhard BN phases by discussing the topological stacking of BN sheets. *c*-BN and *w*-BN can be described by the corrugated BN sheets interconnected by alternating sequence of ABC and A′B′, as shown in figure 1 (a) and (c). According to the structure character of *c*-BN and *w*-BN, a family of new BN phases (named X-BNs hereafter) can be constructed by connecting *c*-BN to *w*-BN along the (0 0 1) and (1 1 1) surface, which is consistent with the experimental results that the polycrystalline BN phase consists of c-BN and w-BN.[5] We find that X-BNs are sp^3-trigonal P3M1 structures. Here, these new phases named X-BNs are labelled by X-$c_{3i}w_{2j}$ (i, j=1, 2.....). *c* and *w* represent

the *c*-BN and *w*-BN, respectively. Subscripts 3*i* and 2*j* represent the number of layers of BN sheets. The number of boron and nitrogen atoms in the conventional smallest unit cell for X-w_2c_3 is 5, as shown in figure 1 (e). We find that all X-BNs phases belong to nH-BN.[18,19,20,21] X-w_2c_3 is the known structure of 5H-BN, which has been synthesized by Komatsu, et al. in experiment.[19] At zero pressure, the conventional unit cell for X-$w_{2i}c_{3j}$ phases have 2*(*i*+*j*) atoms with cell parameter of a=2.56Å, b=2.56Å, c= 2.10*(*i*+*j*). These new phases only contain six-nonplanar rings, which differ from the *pct*-BN[9,12,13] and *Z*-BN.[10] The transition pathway from *h*-BN to X-BN is combination of sliding and buckling of the BN sheets. The naturally staggered, i.e. AB stacked, BN sheets slide along (1 1 0) direction to an aligned AA stacking with the interlayer distance decreasing, and aligned BN sheets deform to form *w*-BN. Similarly, BN sheets B′ slide along (1 -1 0) direction and C′ slide along (1 1 0) direction to form A′B′C′ stacking with the interlayer distance decrasing, which results in the generation of *c*-BN. Besides X-BNs, another family of BN phases (named *L*-BNs hereafter) is proposed. *L*-BNs are constructed by connecting *w*-BN to *w*-BN, as shown in figure 2. The *L*-BNs have the orthorhombic structure. Here, these new phases named L-BNs are labelled by X-w_iw_j (*i*, *j*=1, 2.....). *w* represent the armchair chain, which cut from *w*-BN. Subscripts i and j represent the number of left and right armchair BN chains, respectively. Interestingly, we find that both *pct*-BN and Z-BN belong to our currently proposed family *L*-BNs phases.

The calculated results show that both *X*-BNs and *L*-BNs are stable at zero pressure. The calculated enthalpy value of *L*-BNs is higher than that of *w*-BN, while the enthalpy value of *X*-BNs is lower than that of *w*-BN. X-BNs are more energetically favorable than *w*-BN. In addition, the calculated bulk modulus and densities of *X*-BNs match well with the experimental datas. The *X*-BNs display a transparent wide-gap insulator ground state. Therefore, we assume that the polycrystalline BN phases of high-pressure *h*-BN may consist mainly of *X*-BN with a little other phases, which is consistent with the expermental findings.

All calculations are carried out using density functional theory,[22,23] as implemented in the Vienna *ab initio* simulaiton package (VASP)[24,25] with the projector augmented-wave method employed to describe the electron-ion interaction. The general gradient approximation (GGA) of the Perdew Burke Ernzerhof (PBE) parameterization[26] is adopted to describe the exchange and correlation function. A plane-wave basis set with a cutoff energy 700 eV is used and Monkhorst-Pack[27] k meshes are chosen to ensure that all the enthalpy calculations are well converged to better than 1 meV/atom. Forces on the ions are calculated through the Hellmann-Feynman theorem allowing a full geometry optimization. The electronic structures are calculated by using the screened exchange method (sX-LDA) implemented in CASTEP code.[28] The Thomas-Fermi screening length (k_{TF}) of sX-LDA was determined by evaluating the dynamical average charge density within our newly predicted structures. We took this feature to accomplish the prediction of the electronic structures of the newly determined structures. This is currently unavailable in VASP but we still rely on VASP predicted geometry structures due to its perfect balance between efficiency and accuracy. The XRD patterns for various

structures are porformed by Materials Studio package. The phonon calculations have been carried out by using a supercell approach as implemented in the PHONOPY code.[29]

In order to investigate the relative stabilities of X-BN phases, the enthalpy difference per BN pair with respect to *h*-BN for several allotropes are compared in figure 3 a function of pressure. It is shown that X-BN phases are more favorable than that of *pct*-BN and Z-BN. The enthalpy per BN pair for X-BN phases is between that of *w*-BN and *c*-BN and tends to be the value of *w*-BN and *c*-BN with the increase of *i* and *j*, respectively. The results indicate that X-BN phases have the lowest enthalpy value among all previously proposed BN phases. The calculated enthalpy difference illustrates that the polycrystalline X-BN phases may be the transition phase between *w*-BN and *c*-BN, when *h*-BN is compressed under high pressures.

To further confirm the dynamic stability of X-BN phases, we calculate their phonon band structures by using the supercell method. We take the X-w_2c_3 phase for example, which possesses the smallest unit cell among all X-BN phases and a relatively large interface between the *w*-BN and *c*-BN. The primitive cell for X-w_2c_3 phase contains 10 atoms, giving 30 phonon branches. Around the Γ point, three phonon dispersion curves are observed and no imaginary phonon frequencies are observed in the whole brillouin zone (figure 4 (a)), indicating that the X-w_2c_3 structure is dynamically stable at zero pressure. Similar results are obtained for the other X-BN phases. The calculated results illustrate that X-BN phases are easily achieved in experiment. According to the experimental results, we suggest that the polycrystalline phase of high-pressure *h*-BN is X-BN accompanying with a little other phases. In figure 4 (b), the electronic band structure of X-w_2c_3 is calculated. It is shown that the X-w_2c_3 phase is a wide gap insulator with energy gap Eg=6.12 eV (obtained by sX-LDA), which is lower than that of *w*-BN Eg=6.47 eV and *c*-BN Eg=6.34 eV. Furthermore, the band structure of X-w_8c_3 and X-w_2c_6 phases are calculated. It is shown that from Table 1, the energy gaps of X-w_8c_3 and X-w_2c_6 phases are 6.249 eV and 5.744 eV, respectively. These results show that the energy gaps of polycrystalline BN synthesized from *h*-BN is higher than that of diamond and the polycrystalline BNs are transparent insulators, which can be further confirmed by experiment.

The space group, density, band gap, bulk modulus, shear modulus, Young's modulus and Poisson's ratio of *pct*-BN, *Z*-BN, *w*-BN, *X*-BN and *c*-BN are summarized in Table 1. The calculated lattice parameters (a=b=c=3.625Å) for *c*-BN are consistent well with the experimental results (a=b=c=3.616±0.0005Å and a=b=c=3.615±0.002Å).[16, 30] The calculated density (D=3.458gcm^{-3}) agrees well with the experimental results (D=3.467gcm^{-3}).[16] Furthermore, we obtain bulk modulus (B_0=372.1 GPa) and shear modulus (G=387.6 Gpa) for *c*-BN phase, which matchs well with the experimental datas (B_0=369±14 GPa and G=391 Gpa).[16] The further study shows that X-BN phases are denser than that of *pct*-BN and Z-BN, and their densities are comparable to those of *w*-BN and *c*-BN. Additionally, the bulk modulus, shear modulus, Young's modulus and Poisson's ratio for X-BN phases are comparable to those of *w*-BN and *c*-BN. The calculated results futher indicate that the polycrystalline phases of high-pressure *h*-BN may be *X*-BN phase, which is mainly

constructed from *c*-BN and *w*-BN at a certain proportion.

Finally, the XRD patterns of *w*-BN, *c*-BN and X-BN phases have been simulated in order to instructing the experiment. At the zero pressure, the simulated intensive peak position and relative intensities of *w*-BN and *c*-BN match the experimental results very well.[16] As we know that each phase has its own characteristic peaks, which correspond to different crystal plane, as shown in figure 5 (a) and (b). For X-BN phases, the XRD patterns are almost the superposition of *w*-BN and *c*-BN. In addition, the different characteristic peaks are observed in XRD patterns. Thus, the nano-polycrystalline structure of X-BN phases, constructed from *w*-BN and *c*-BN, can be further identified according to the additional characteristic peaks, which presents important theoretical guidance for the experiment and can help us understand the structural phase transition of high-pressure *h*-BN.

In conclusion, two classes of structural families of boron nitride allotropes are proposed. We find that the previously proposed *pct*-BN, *Z*-BN belong to our currently proposed family *L*-BNs. The *X*-BNs have the lowest enthalpy value amony all proposed BN phases.The transition from *h*-BN to *X*-BNs can occur simply through sliding and buckling of BN sheets. The electronic bonding indicates that X-BNs possess covalent character with sp^3-hybridized electronic states. The calculated band structure shows that the energy gaps of X-BNs are larger than 5 eV, indicating X-BNs transparent superhard materials. We hope that the family of X-BN phases can help us understand the lattice structure of polycrystalline BNs and phase transition mechanism of high-pressure *h*-BN.

Acknowledgements

This work was supported by the National Natural Science Foundation of China (Grant No. 11174242, 11204265), the Natural Science Foundation of Jiangsu Province (Grant No. BK2012248), the fund of Key Laboratory for Advanced Technology in Environmental Protection of Jiangsu Province (Grant No. AE201021).

References

(1) A. Y. Liu, M. L. Cohen, *Science* **1989**, **245**, 841-842.
(2) D. M. Teter, R. J. Hemley, *Science* 1996, **271**, 53-55.
(3) R. B. Kaner, J. J. Gilman, S. H. Tolbert, *Science* 2005, **308**, 1268-1269.
(4) V.V. Brazhkin, A. G. Lyapin, R. J. Hemley, *Philos. Mag. A* 2002, **82**, 231-253.
(5) N. Dubrovinskaia, L. Solozhenko, N. Miyajima, V. Dmitriev, O. O. Kurakevych, L. Dubrovinsky, *Appl. Phys. Lett.* 2007, **90**, 101912-101914.
(6) Y. Zhang, H. Sun, C. F. Chen, *Phys. Rev. Lett.* 2005, **94**, 145505-145508.
(7) Y. Zhang, H. Sun, C. F. Chen, *Phys. Rev. B* 2006, **73**, 144115-144121.
(8) R. F. Zhang, S. Veprek, A. S. Argon, *Phys. Rev. B* 2008, **77**, 172103-172106.
(9) Z. P. Li, F. M. Gao, *Phys. Chem. Chem. Phys.,* 2012, **14**, 869–876.
(10) C. Y. He, L. Z. Sun, C. X. Zhang, X. Y. Peng, K. W. Zhang, J. X. Zhong, *Phys. Chem. Chem. Phys.,* 2012, **14**, 10967–10971.
(11) Z. C. Pan, H. Sun, Y. Zhang, C. F. Chen, *Phys. Rev. Lett.* 2009, **102**, 55503-055506.
(12) B. Wen, J. J. Zhao, R. Melnik, Y. J. Tian, *Phys. Chem. Chem. Phys.,* 2011, **13**, 14565–4570.

(13) L. Hromadováň, R. Martoňák, *Phys. Rev. B,* 2011, **84**, 224108–224144.
(14) H. Sumiya, S. Uesaka, S. Satoh, *J. Mater. Sci.* 2000, **35**, 1181-1186.
(15) H. Sumiya, S. Uesaka, *J. Jpn. Soc. Powder Metall.* 2002, **49**, 327-332.
(16) A. Nagakubo, H. Ogi, H. Sumiya, K. Kusakabe, M. Hirao, *Appl. Phys. Lett.* 2013, **102**, 241909-241914.
(17) Y. Ishida, H. Sumiya, in Proceedings of the 2012 Powder Metallurgy World Congress & Exhibition, edited by H. Miura and A. Kawasaki, 18D-T13-28 (The Japan Society of Powder and Powder Metallurgy, Yokohama, 2012).
(18) A. R. Verma and P. Krishna, "Polymorphism and Polytypism in Crystals" (Wiley, New York, 1966).
(19) S. Komatsu, K. Okada, Y. Shimizu, and Y. Moriyoshi: J. Phys. Chem. B 103 (1999) 3289.
(20) K. Kobayashi and S. Komatsu: J. Phys. Soc. Jpn. 2007, 76, 113707-113710.
(21) K. Kobayashi and S. Komatsu: J. Phys. Soc. Jpn. 2008, 77, 084703-084712.
(22) Chunyi Zhi, Yoshio Bando, Chengchun Tang, and Dmitri Golber Phys. Rev. B 2005, 72, 245419-245423
(23) Chunyi Zhi, Yoshio Bando, Chengchun Tang, and Dmitri Golber Phys. Rev. B 2006, 74, 153413-153416
(24) G. Kresse, J. Furthmüller, *Phys. Rev. B*, 1996, **54**, 11169–11186.
(25) G. Kresse, J. Furthmüller, *Comput. Mater. Sci.,* 1996, **6**, 15–50.
(26) J. P. Perdew, K. Burke, M. Ernzerhof, *Phys. Rev. Lett.*, 1996, **77**, 3865–3868.
(27) H. J. Monkhorst, J. D. Pack, *Phys. Rev. B*, 1976, **13**, 5188–5192.
(28) S. J. Clark, M. D. Segall, C. J. Pickard, P. J. Hasnip, M. I. J. Probert, K. Refson, M. C. Payne, *Z. Kristallogr.* 2005, **220**, 567–570.
(29) K. Parlinski, Z. Q. Li, Y. Kawazoe, *Phys. Rev. Lett.,* 1997, **78**, 4063–4066.
(30) E. Knittle, R. M. Wentzcovitch, R. Jeanloz, M. L. Cohe, *Nature*, 1989, **337**, 349–352

Figure caption:

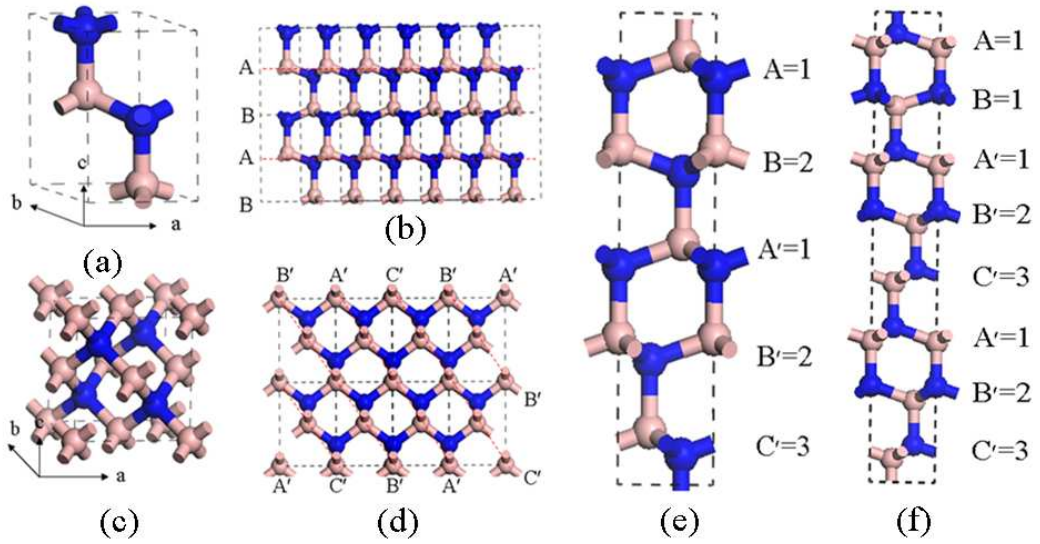

Figure 1. (a) and (c) illustrate the crystallographic structure of the w-BN and c-BN. (b) and (d) show the 2D projections of the 6×1×2 supercell of w-BN along (1, 1, 0) direction and of the 3×2×1 supercell of c-BN along (1, 0, 1) direction. (e) and (f) show the 2D projections of the unit cell of X-c_3w_2 and X-c_6w_2 respectively.

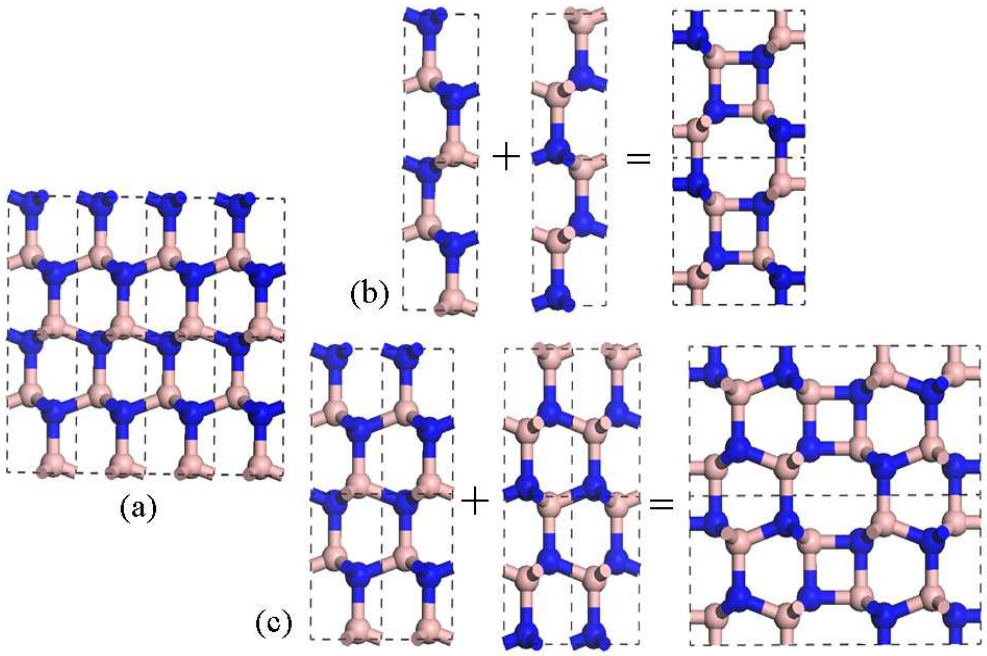

Figure 2. (a) shows the 2D projections of the 4×1×2 supercell of w-BN along (1, 1, 0) direction. (b) and (c) show the combination of the X-w_1w_1 BN phase and X-w_2w_2 BN phase, respectively.

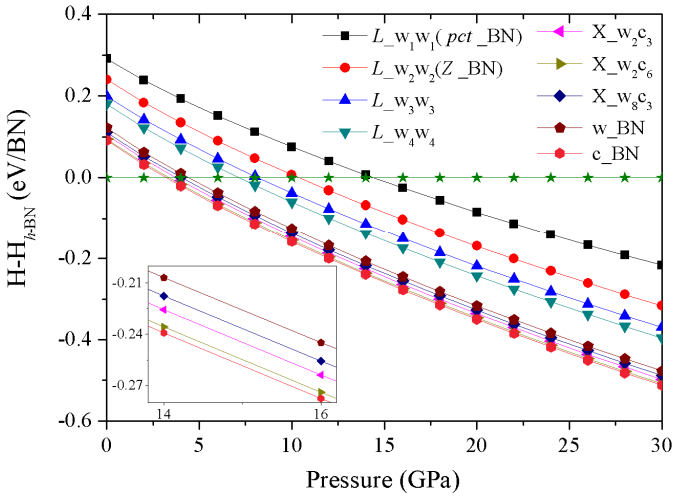

Figure 3. Calculated enthalpy difference per BN pair with respect to *h*-BN for numerous BN allotropes versus pressure.

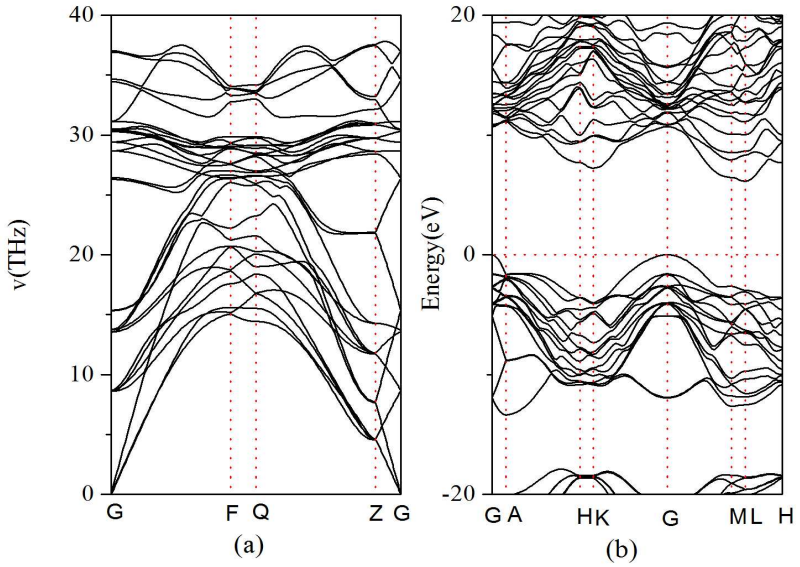

Figure 4. Properties of the X-w_2c_3 phase (a) Calculated phonon dispersion curves of X-w_2c_3 phase at 0 GPa. (d) Calculated electronic band structure at zero pressure.

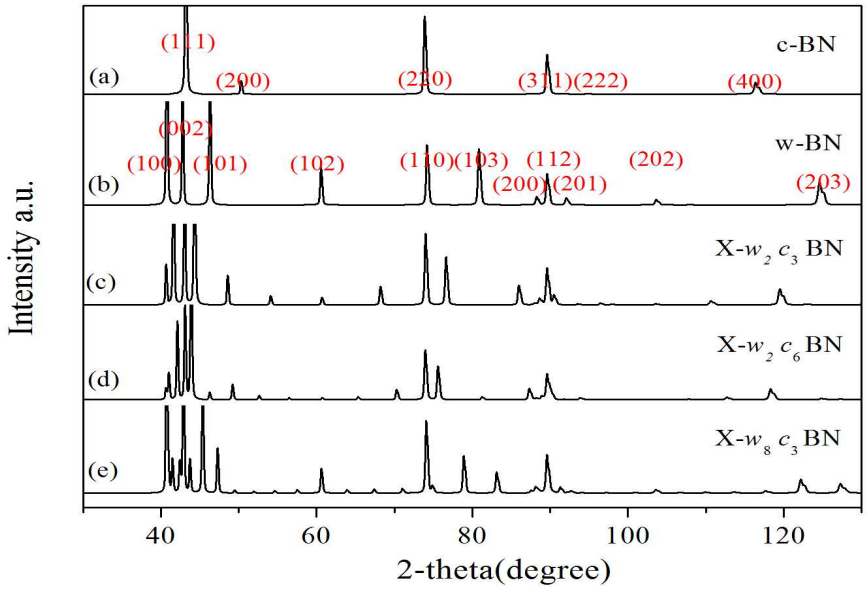

Figure 5. The simulated XRD patterns of *w*-BN, *c*-BN and X-BNs.

Table 1 – Space group, lattice parameters (LP), density (D: gcm^{-3}), band gap (E_g:eV), bulk modulus (B_0: GPa), shear modulus (G: GPa), Young's modulus (Y: GPa), and Poisson's ratio (ν) for pct-BN, Z-BN, *w*-BN, X-BN and c-BN

Systems	Space group	LP	D	E_g	B_0	G	Y	ν	Ref
XL-BN(1)	*P4$_2$/mnm*	a=b=4.425Å, c=2.550Å	3.301		348.9	314.8	726.1	0.1532	This work
		a=b=4.425Å, c=2.548Å	3.431		348.4	309.4			
		a=b=4.380Å, c=2.526Å			349.7				
XL-BN(2)	*Pbam*	a=8.893Å, b=4.294Å, c=2.556Å	3.379		355.3	348.5	787.9	0.1304	This work
		a=8.891Å, b=4.293Å, c = 2.555Å	3.52		359.6	347.5			Calculated[10]
XL-BN(3)	*Pnnm*	a=13.317Å, b=4.267Å, c=2.556Å	3.404		361.3	361.4	813.2	0.1249	This work
XL-BN(4)	*Pbam*	a=17.744Å, b=4.257Å, c=2.556Å	3.416		363.8	367.3	824.4	0.1223	This work
w-BN	*P6$_3$mc*	a=b=2.555 Å, c=4.225Å	3.451	6.47	371.8	386.6	861.3	0.1140	This work
		a=b=2.538 Å, c=4.197Å	3.587	5.24	375.2	384.2			Calculated[10]
		a=b=2.55 Å, c=4.20Å	3.467						Experiment[16]
X-w$_2$c$_3$ BN	*P3M1*	a=b=2.56Å, c=10.5Å	3.455	6.12	370.9	386.2	860.1	0.1136	This work
X-w$_8$c$_3$ BN	------	a=b=2.56Å, c=16.78Å	3.452	5.74	372.0	387.0	862.1	0.1376	This work
X-w$_2$c$_6$ BN	------	a=b=2.56Å, c=23.18Å	3.457	6.25	371.9	386.1	860.5	0.1144	This work
c-BN	*F-43m*	a=b=c=3.625Å	3.458	6.34	372.1	387.6	863.2	0.1135	This work
		a=b=c=3.625Å	3.593	4.40	376.2	381.5			Calculated[10]
		a=b=c=3.616±0.0005Å	3.467			391			Experiment[16]
		a=b=c=3.615±0.002Å			369±14				Experiment[24]